Estimation of Precipitating Electron Energy of Pulsating Aurora Using Ground-based Multiwavelength Optical Observations

K. Toyama[1], Y. Miyoshi[1], S. Kurita[2], K. Hosokawa[3], Y. Ogawa[4], S. Oyama[1,4,7], S. Saito[5], K. Shiokawa[1], K. Asamura[6], T. Asano[1], F. Tsuchiya[8] , and R. Fujii[1],

[1]Insitute for Space-Earth Environmental Research, Nagoya University, Nagoya, Japan

[2]Research Institute for Sustainable Humanosphere, Kyoto University, Uji, Japan

[3]The University of Electro-Communications, Chofu, Japan

[4]National Institute for Polar Research, Tachikawa, Japan

[5]National Institute of Information and Communication Technology, Koganei, Japan

[6]Institute of Space and Astronautical Science, Japan Aerospace Exploration Agency, Sagamihara, Japan

[7]Space Physics and Astronomy Research Unit, University of Oulu, Oulu, Finland

[8]Planetary Plasma and Atmospheric Research Center, Tohoku University, Sendai, Japan

Corresponding author: Yoshizumi Miyoshi (miyoshi@isee.nagoya-u.ac.jp)

Key Points:

- The precipitating electron energy of pulsating aurorae is estimated using images from all-sky cameras with narrow-band optical filters.

- Spatial distribution of precipitating electron energies is not uniform in the pulsating auroral (PsA) patch.
- The coherent spatial scale of the wave-particle interactions is smaller than each PsA patch size.

Abstract

Pulsating aurora (PsA) is characterized by quasi-periodic intensity modulations with a period of a few to a few tens of seconds. It is caused by precipitation of energetic electrons of a few to several tens of kilo electronvolts produced by chorus waves in the magnetosphere. Precipitating electron energies of PsA have been identified in the past by sounding rocket and satellite observations, but the spatial distributions of precipitating electron energies of PsA have never been estimated. In this study, using the data from ground-based all-sky cameras at two wavelengths of 427.8 nm and 844.6 nm, we estimated the temporal and spatial variations in the precipitating electron energy of PsA. The results showed that the spatial distribution of precipitating electron energies was not uniform in the PsA patch, suggesting that the coherent spatial scale of the wave-particle interactions is smaller than each PsA patch size.

Plain Language Summary

Pulsating aurora (PsA) is caused by the intermittent electron precipitation at an energy range from a few kilo-electronvolt to tens of kiloelectronvolt through electron interactions of chorus waves. Previous sounding rocket and satellite observations have detected the precipitating electrons of PsA, but spatial distributions of precipitating electrons inside the PsA patch have not been derived. The purpose of this study is to determine the variations of the characteristic energy and downward energy flux, using ground-based all-sky cameras with multi-wavelength observations. The results showed that the precipitating electron energy and downward energy flux are not uniform in the PsA patch, suggesting that the coherent spatial scale of the wave-particle interactions is smaller than each PsA patch size.

1. Introduction

[1] Pulsating aurora (PsA) is a type of diffuse aurora, which is typically observed between midnight and dawn during the recovery phase of a substorm (e.g., Lessard, 2012, Hosokawa et al., 2015, Nishimura et al., 2020). Pulsating aurorae exhibit two characteristic temporal variations: the main pulsation, which is a quasi-periodic modulation lasting from a few seconds to a few tens of seconds, and the internal modulation, which is a modulation of a few hertz embedded within the main pulsation (e.g., Miyoshi et al., 2010, 2015). Pulsating aurorae are caused by electrons that precipitate into the atmosphere due to pitch-angle scattering by chorus waves in the magnetosphere (e.g., Nishimura et al., 2010; Miyoshi et al., 2015, 2020, 2021; Kasahara et al., 2018; Hosokawa et al., 2020).

[2] Sounding rocket and satellite observations have ascertained that energetic electron fluxes of a few to several tens of kilo-electronvolt produce pulsating aurorae (Bryant et al., 1975; Sandahl et al., 1980; Miyoshi et al., 2010). Miyoshi et al. (2015) proposed a model in which lower-band chorus (LBC) bursts cause the main modulations of PsA, and rising tone elements embedded in an LBC burst cause the internal modulations. The mechanisms are confirmed by the recent conjugate observations by the Arase satellite and a ground-based high-speed Electron-Multiplying CCD (EMCCD) camera (Hosokawa et al., 2020).

[3] Ground-based optical observations have been used to estimate the precipitating electron energy of PsA. Ono (1993) estimated the precipitating electron energy of PsA using observations from a multi-wavelength photometer with an intensity ratio of 427.8 to 844.6 nm. He demonstrated that the estimated energy for the main pulsation is a few kilo-electronvolt. While ground-based optical imaging observations at multiple wavelengths are useful for determining the spatial distributions of the precipitating electron energy of aurora (Grubbs et al., 2017), such imaging observations have not been done for the study of PsA. Using the color digital cameras onboard the International Space Station (ISS), Nanjo et al. (2021) estimated the ratio of blue to green (B/G ratios) that are proxies for the energies of PsA electrons. They found that the B/G ratio tends to be higher in the morning sector than in the midnight sector, which is consistent with the results of previous studies showing the MLT dependence of the energies of PsA electrons (e.g., Hosokawa and Ogawa, 2015; Paratamies et al., 2017).

[4] The in-situ observations of sounding rockets (Sandahl et al., 1980; Yau et al., 1981) and low-altitude satellites (Miyoshi et al., 2010, 2015) can provide the detailed energy spectrum of precipitating electrons during PsA appearance, but these observations are limited to a point inside the PsA patch. In general, PsA exhibits dynamic spatio-temporal variations during pulsations (Nishimura et al., 2020). Nishiyama et al. (2016) reported on the sub-patch structures of each PsA patch, suggesting that coherent chorus-wave particle interaction regions are smaller than those of each PsA patch. Therefore, it is important to investigate the two-dimensional (2D) spatio-temporal variations of the precipitating electrons within a PsA patch using ground-based observations to understand the detailed electron scattering mechanisms creating PsA. The purpose of this study is to determine variations of the characteristic energy and downward energy flux of PsA through space and time, using ground-based all-sky cameras with multi-wavelength observations. In this study, we develop a method to derive the characteristic energy and downward energy flux of PsA from multi-wavelength observations and a two-stream simulation of precipitating electrons, and we apply the method to the actual PsA event.

2. Methods and Observations

[5] To understand spatio-temporal variations in the precipitating electron energy of PsA, we estimate the precipitating electron energy using images taken from a couple of newly installed all-sky cameras at two wavelengths with narrow-band optical filters. From an analysis with a two-stream simulation of production of optical emissions by precipitating electron fluxes (Solomon, 2017), we obtain the characteristic energy of precipitating electrons from the optical observation and derived their spatio-temporal variations.

[6] We operated two high-speed all-sky imagers (ASIs) in Tromsø, Norway (69.6ºN, 19.2ºE in geographic coordinates). Two ASI systems consist of a fish-eye lens, narrow-band optical filters at 427.8 and 844.6 nm (Taguchi et al., 2004), and EMCCD camera systems (Hosokawa et al., 2021). These wavelengths were selected after detail considerations about the possible wavelength for the optical measurements (Oyama et al., 2018). The EMCCD detector images had a sampling frequency of 10 Hz and a spatial resolution of 256 × 256 CCD pixels. The field of view (FOV) was approximately 500 × 500 km at an altitude of 110 km. The two ASI systems

were calibrated using an optical calibration system at the National Institute of Polar Research (NIPR), Japan, to derive their absolute sensitivity (Ogawa et al., 2020).

[7] Using the data collected in our observations, we calculated the absolute intensity of the auroral emission at each wavelength by subtracting the EMCCD dark counts. This absolute intensity contains both actual PsA emissions as well as other background auroral emissions. We consider the background auroral emission intensities as running averages of absolute intensities over 10 s at each pixel. To estimate the actual PsA emissions , we subtracted the running averages from the absolute intensities at each pixel at each time. The ratio of the estimated energy with and without this subtraction of running averages at the magnetic zenith was 1.5 in this study, suggesting that the calculation of energy without background subtraction causes systematic underestimation of the actual precipitating energy. Because the van Rhijn effect becomes significant at a large zenith angle (Kubota et al., 2001), we used data with a zenith angle smaller than 30°. The attenuations due to the combination of atmospheric extinction and the van Rhijin effect at zenith angle 30° are 1.03, and 0.93 if the atmospheric extinction factor is 0.1 and 0.2, respectively.

[8] As in previous studies (e.g., Ono, 1993), we estimated the intensity ratio of PsA at two wavelengths to determine the precipitating electron energy. We first derived the expected ratio of optical emissions at two wavelengths as a function of the precipitating electron energies, using the two-stream simulation by the GLobal airglOW model (GLOW) (Solomon, 2017). Same method has been applied for the discrete aurora (Grubbs et al., 2017).

[9] We also evaluated the uncertainty of the estimated energies by considering the error propagation. This uncertainty is caused by the statistical error of the observed count of the EMCCD and the error of the intensity ratio-energy conversion obtained from GLOW. From these two errors, the average uncertainty is 54% in the magnetic zenith direction during the period of this study.

3 Results

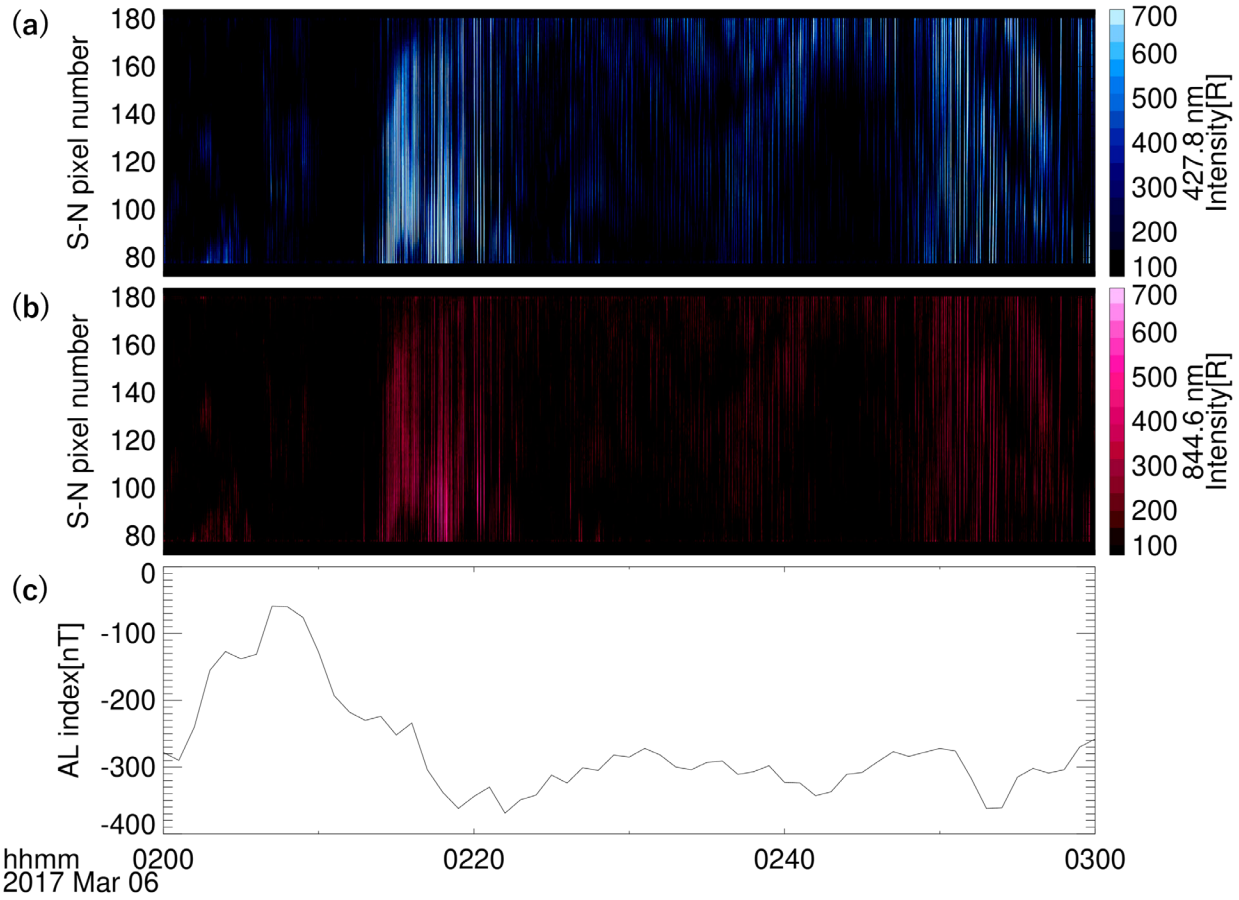

Figure 1. Keograms of pulsating auroral emissions for (a) 427.8 and (b) 844.6 nm observed at Tromsø, Norway, and (c) the AL index on March 6, 2017/02:00:00-03:00:00 UT.

[10] **Figure 1** shows the keograms at 427.8 and 844.6 nm from 02:00 to 03:00 Universal Time (UT) (04:30 to 05:30 Magnetic Local Time [MLT]) on March 6, 2017. The bottom panel shows the AL index, indicating a moderate substorm occurred during this interval. The substorm onset was 02:07 UT. At approximately 02:15 UT and 02:50 UT, significant PsA emissions were observed during the substorm expansion and recovery phase. The average pulsation period of the main pulsation during this time interval was 11.2 ± 7.1 s, and the average emission intensity in the main pulsation was about 320 ± 200 and 160 ± 80 Rayleigh (R) at 427.8 and 844.6 nm, respectively.

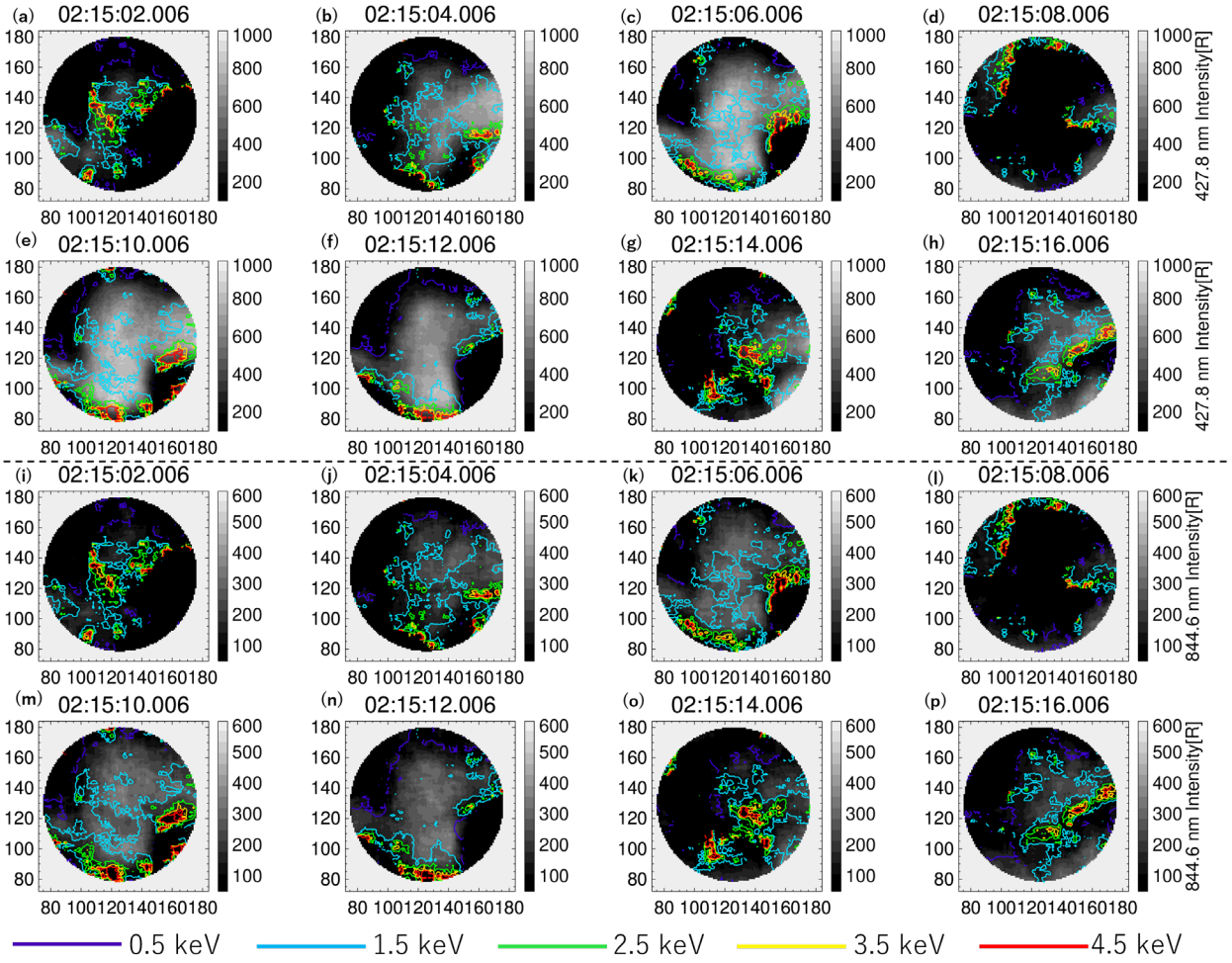

Figure 2. All-sky images of pulsating auroral patches at (a)-(h) 427.8 nm and (i)-(p) 844.6nm observed at Tromsø, Norway, from 02:15:02 to 02:15:16 UT on March 6, 2017 (zenith angle less than 30°). Contours of estimated characteristic energies are also shown in color. Light blue, green, yellow, and red contours indicate 1.5, 2.5, 3.5, and 4.5 keV, respectively.

[11] **Figure 2** shows the all-sky images of the pulsating auroral patches at 427.8 nm observed at Tromsø, Norway, from 02:15:02 to 02:15:16 UTC with superposed contours of the estimated energy in color (1.5, 2.5, 3.5, and 4.5 keV). During this time interval, a patch of PsA was clearly identified within the FOV of ASI. The PsA patch shows three main pulsations. The patch expanded from east to west, and its size was approximately 200 and 110 km in the east-west and north-south direction, respectively, assuming an emission altitude of 110 km.

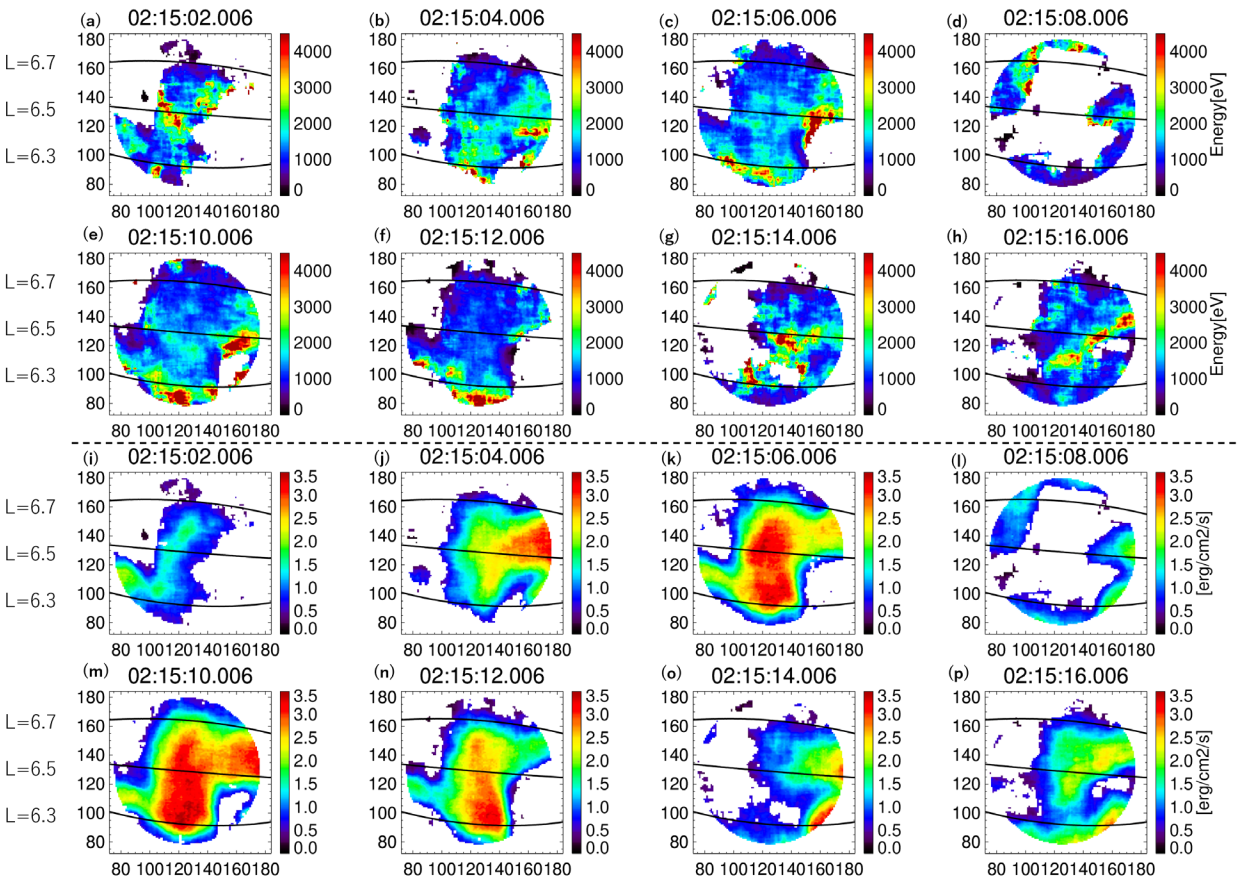

Figure 3. Two-dimensional distribution of estimated characteristic energies (a-h) and downward energy fluxes (i-p) at zenith angles less than 30° from 02:15:02 to 02:15:16 UT on March 6,2017. These images are at the same time interval as the images in Figure 2. Three black lines in each plot indicate the L values of L = 6.7, 6.5, and 6.3, from top to bottom.

[12] **Figure 3** shows the 2D distribution of the estimated energies and downward energy fluxes for the same time interval as that in Figure 2. The pixels with 427.8-nm intensity less than 100 R or 844.6-nm intensity less than 50 R were eliminated because of the small signal/noise ratio. During the ON times (02:15:06 and 02:15:10UTC), high-energy electrons of more than 1.5 keV precipitated into the center of the patch. However, the precipitating electron energies around the PsA patch was small (~1 keV). The average estimated energy and the average downward energy

143 flux for the pulsating ON time at the magnetic zenith were 1.54 keV and 2.32 erg/cm^2/s,
144 respectively.

145 [13] We derived the L-shells at a 110-km altitude using the Altitude Adjusted Corrected
146 Geomagnetic Model (AACGM, Baker and Wing, 1989), as shown in **Figure 3**. **Table 1** shows
147 the average energies inside the patches at L = 6.3, 6.5, and 6.7 for the consecutive three main
148 pulsations ON times. The statistical t-test confirmed the significance of this L-shell dependence
149 of the precipitating electron energies at the first two pulsations, while no significance at the last
150 pulsation. As shown in **Figure 3** (i-p), the size of the last patch is smaller than the two preceding
151 patches, which may be a reason for no significant dependence. The precipitating electron energy
152 depended on the location of the PsA patch. For the first two ON times, the energy in the lower L-
153 shell (L = 6.3) was higher than that in the higher L-shell (L = 6.7).

154 **4 Summary and Discussion**

155 [14] In this study, we developed the method to derive precipitating electron energies using two-
156 wavelength observations and determined, for the first time, the 2D spatial distributions of the
157 precipitating electron energies during PsA. These spatio-temporal variations of PsA have not
158 been detected previously by single-point observations, such as those of sounding rockets and
159 low-altitude satellites. The 2D imaging optical observations with two wavelengths have a
160 significant advantage for deriving the fundamental characteristics of precipitating electrons,
161 especially for the spatial distributions of precipitating electrons of PsA.

162 [15] We investigated the PsA event at Tromsø, Norway, that occurred during the substorm
163 expansion and recovery phase on March 6, 2017. The minimum AL index was -369 nT. Our
164 findings show that the average energy increased during the pulsating ON time, reaching 1.54
165 keV at the magnetic zenith, which is consistent with the previous study that observed a point
166 inside PsA patch using the photometer (Ono, 1993). Further, we determined the spatio-temporal
167 evolutions of the precipitating electron energy. We found that the characteristic energy and
168 downward energy flux of precipitating electrons inside the PsA patch were not uniform. The
169 results revealed that the precipitating electrons increased at the lower L-shell at 02:15:03 UTC
170 and 02:15:08 UTC, while they were nearly the same at 02:15:13 UT.

[16] The typical spatial scale of the coherency of the chorus waves is ~960 km (0.15 Re) in the magnetosphere (Agapitov et al., 2021). If we map this scale to the ionosphere, it will become ~100 km in latitudes which is smaller than the scale size of pulsating auroral patches for the present event. Thus, it is expected that the precipitating electron energy has a spatial distribution inside a PsA patch. A principal component analysis has reported that the PsA patch consists of several sub-patch structures (Nishiyama et al., 2016). They showed that the average spatial scale of sub-patches is ~800 km at the magnetic equator, which is consistent with the coherence scale of the chorus waves. Our findings shown in Table 1 indicate that the precipitating electron energy is not uniform in the spatial scale of ~1300 km (L-value difference of 0.2); thus, these spatial structures of precipitating electrons indicate the non-uniform wave-particle interactions inside the PsA patch.

Acknowledgments:

This work is conducted with funding from Grants-in-Aid for JSPS (15H05747, 16H06286, 20H01959, 20H01955, 21H04526, 21KK0059, 21H04518, 21K18651, JPJSBP120194814).

Open Research:

The EMCCD camera data used in this study are available at the ERG-Science Center (Miyoshi et al., 2018). The 427.8 nm (https://doi.org/10.34515/DATA.GND-0059-0006-0205_v01) and the 844.6 nm (https://doi.org/10.34515/DATA.GND-0059-0006-0203_V01) are used.

References

Baker, K. B. and S. Wing (1989), A new magnetic coordinate system for conjugate studies at high latitudes, *J. Geophys. Res.*, 94(a7), p. 9139, doi:10.1029/JA094iA07p09139.

196 Bryant, D., M. J., Smith, and G. M., Courtier (1975), Distant modulation of electron intensity during the expansion
197 phase of an auroral substorm, *Planet. Space. Sci.*, 23(5), 867-878. https://doi.org/10.1016/0032-0633(75)90022-7
198
199 Grubbs, G., R. Michell, M. Samara, D. Hampton, and J.-M. Jahn (2016), Predicting Electron Population
200 Characteristics in 2-D Using Multispectral Ground-Based Imaging, *Geophys. Res. Lett.*, 45(1), 15-20.
201 https://doi.org/10.1002/2017GL075873
202
203 Hosokawa, K, Y. Miyoshi, and W. Li (2015), Introduction to Special Section on Pulsating Aurora and Related
204 Magnetospheric Phenomena, *J. Geophys. Res.*, 120, doi:10.1002/2015JA021453.
205 Hosokawa, K., and Y. Ogawa (2015),Ionospheric variation during pul-sating aurora,*J. Geophys. Res.Space*
206 *Physics*,120, 5943–5957,doi:10.1002/2015JA021401
207
208 Hosokawa, K., Y. Miyoshi, et al. (2020), Multiple time-scale beats in aurora: precise orchestration via
209 magnetospheric chorus waves, *Sci. Reports,* 10, 3380. https://doi.org/10.1038/s41598-020-59642-8
210
211 Hosokawa, K., Oyama, S., et al. (2021), A ground-based instrument suite fo integrated high-time resolution
212 measurements of pulsating aurora with Arase, *Earth and Space Science Open Archive*.
213 https://doi.org/10.1002/essoar.10504721.1" https://doi.org/10.1002/essoar.10504721.1
214
215 Kasahara, S., Miyoshi, et al. (2018), Pulsating aurora from electron scattering by chorus waves, *Nature*, 554, 337-
216 340. https://doi.org/10.1038/nature25505
217
218 Kennel, C. F., and H. E. Petschek (1966), Limit on stably trapped particle fluxes, *J. Geophys. Res.*, 71(1), 1–28.
219 https://doi.org/10.1029/JZ071i001p00001
220
221 Kubota, M., H. Fukunishi, and S. Okano, (2001), Characteristics of medium- and large-scale TIDs over Japan
222 derived from OI 630-nm nightglow observation, *Earth, Planets and Space*, 53(7), 741-751.
223 https://doi.org/10.1186/BF03352402

Lessard, M. (2012), A review of pulsating aurora, in Auroral Phenomenology and Magnetospheric Processes: Earth and Other Planets, edited by A. Keiling et al., Geophys. Monogr. Ser., 197, 55–68, doi:10.1029/2011GM001187.

Miyoshi, Y., Hosokawa, et al. (2021), Penetration of MeV electrons into the mesosphere accompanying pulsating aurorae, *Sci. Reports*, 11, 13724. https://doi.org/10.1038/s41598-021-92611-3

Miyoshi, Y., Katoh, Y., et al. (2010), Time of flight analysis of pulsating aurora electrons, considering wave-particle interactions with propagating whistler mode waves, *J. Geophys. Res.*, 115, A10312. https://doi.org/10.1029/2009JA015127

Miyoshi, Y., S. Saito, et al. (2015), Relation between fine structure of energy spectra for pulsating aurora electrons and frequency spectra of whistler mode chorus waves, *J. Geophys. Res.*, 120(9), 7728-7736. https://doi.org/10.1002/2015JA021562

Miyoshi, Y., T. Hori, et al.(2018), The ERG Science Center, Earth, Planets, Space., 70:96, doi:10.1186/s40623-018-0867-8.

Miyoshi, S. Saito et al.(2020), , Relativistic Electron Microbursts as High Energy Tail of Pulsating Aurora Electrons, Geophys. Res. Lett., 47 doi:10.1029/2020GL090360,2020.

Nanjo, S., Y. Hozumi, K. Hosokawa, R. Kataoka, Y. Miyoshi, S-I. Oyama, et al. (2021). Periodicities and colors of pulsating auroras: DSLR camera observations from the International Space Station, *J. Geophys. Res.*, 126, e2021JA029564, https://doi.org/10.1029/2021JA029564/

Nishimura, Y., M. R. Lessard, et al. (2020), Diffuse and pulsating aurora, *Space Sci. Rev.*, 216(4), https://doi.org/10.1007/s11214-019-0629-3

Nishiyama, T., Miyoshi, Y. et al.(2016), Substructures with luminosity modulation and horizontal oscillation in pulsating patch: Principal component analysis application to pulsating aurora, *J. Geophys. Res.*, 119, 3514-3527. https://doi.org/10.1002/2014JA019818

Ogawa, Y., A. Kadokura, A., and M. K. Ejiri (2020), Optical calibration system for NIPR for aurora and airglow observations, *Polar Sci.*, 26. https://doi.org/10.1016/j.polar.2020.100570

Ono, T., (1993), Derivation of energy parameters of precipitating auroral electrons by using the intensity ratios of auroral emissions, *J. Geomag. Geoelectric.*, 45(6), 455–472. https://doi.org/10.5636/jgg.45.455

Oyama, S., T. T. Tsuda, K. Hosokawa, Y. Ogawa, Y. Miyoshi, S. Kurita, A. E. Kero, R. Fujii, Y. Tanaka, A. Mizuno, T. Kawabata, B. Gustavsson, and T. Leyser (2018), Auroral molecular-emission effects on the atomic oxygen line at 777.4 nm, *Earth, Planet and Space,* 70:166, doi:10.1186/s40623-018-0936-z.

Partamies, N., D. Whiter, A. Kadokura,K. Kauristie, H. Nesse Tyssøy, S.Massetti, P. Stauning, and T. Raita(2017), Occurrence and average behav-ior of pulsating aurora,*J. Geophys.Res. Space Physics*,122, 5606–5618,doi:10.1002/2017JA024039

Sandahl, I., L. Eliasson, and R. Lundin, (1980), Rocket observations of precipitating electrons over a pulsating aurora, *Geophys. Res. Lett.*, 7(5), 309–312. https://doi.org/10.1029/GL007i005p00309

Solomon, S. C., (2017), Global modeling of thermospheric airglow in the far ultraviolet, *J. Geophys. Res.*, 122(7), 7834–7848. https://doi.org/10.1002/2017JA024314

Taguchi, M., M. Ejiri, M., and K. Tomimatsu, (2004), A new all-sky optics for aurora and airglow imaging, *Adv. Polar Upper Atmos. Res*., 18, 140-148.

279

280 **Table 1.** Average energy of PsA on time at each L value

UT	L = 6.7	L = 6.5	L = 6.3
02:15:03-08	1.22 keV	1.56 keV	2.68 keV
02:15:08-13	1.04 keV	1.49 keV	3.77 keV
02:15:13-16	1.39 keV	1.58 keV	1.20 keV

281

282

283

284